Int. J. Industrial. Model. chem. 2025; 16(2) 1-14

International Journal of Industrial Chemistry (IJIC)

https://doi.org/10.57647/j.ijic.2025.1602.12

Design of Temperature-Sensitive Hydrogel Nanoparticles and Investigation of Their Application in the Development of a New Generation of Anti-Cancer Drugs with Optimization Conditions by Central Composite Design

Baharak Tavassoty Kheiry[1], Fariba Tadayon[1*], Homayon Ahmad Panahi[2], Elham Moniri[3]

[1] *Department of Chemistry, NT.C., Islamic Azad University, Tehran, Iran*

[2] *Department of Chemistry, Central Tehran Branch, Islamic Azad University, Tehran, Iran*

[3] *Department of Chemistry, Varamin (Pishva) Branch, Islamic Azad University, Varamin, Iran*

***Corresponding author:** Fariba.tadayon@iau.ac.ir

Research Article

Received:
10 March 2025

Revised:
8 May 2025

Accepted:
29 May 2025

Published in Issue:
30 June 2025

Abstract

Temperature-sensitive nanohydrogels present notable advantages in biomedical applications due to their high permeability, selectivity, water solubility, and minimal invasiveness, making them ideal carriers for controlled chemotherapy drug delivery. In this study, a novel polyphenylglycine-based nanohydrogel was synthesized via N-phenylglycine polymerization and subsequently functionalized with heat-responsive and allylamine groups to improve solubility and introduce additional active sites. The multi-target anticancer drug, sunitinib malate (Sun), was then incorporated into the nanohydrogel for targeted delivery. The structure of the nanohydrogel was confirmed via FTIR, XRD, FE-SEM, EDX, and TGA analyses. Drug loading parameters, including pH, contact time, and temperature, were optimized using response surface methodology, yielding optimal conditions at pH 7.4, 60 minutes, and 50 °C. Adsorption followed the Langmuir isotherm (19.81 mg/g monolayer capacity), and the kinetics were best described by a pseudo-second-order model. The nanohydrogel exhibits a lower critical solution temperature slightly above physiological temperature and demonstrates excellent photothermal stability. These properties highlight its potential as a promising platform for controlled and targeted delivery of anti-cancer therapeutics.

Keywords: Nanohydrogels, Temperature-Sensitive, Photothermal Polymer, Drug Delivery, Sunitinib Malate, Chemotherapy

Cite this article: Tavassoty Kheiry B.,Tadayon F., Ahmad Panahi H., Moniri E. (2025). Design of Temperature-Sensitive Hydrogel Nanoparticles and Investigation of Their Application in the Development of a New Generation of Anti-Cancer Drugs with Optimization Conditions by Central Composite Design. , *International Journal of Industrial Chemistry,* 16(2). 1-14. https://doi.org/10.57647/j.ijic.2025.1602.12

1. Introduction

In recent decades, nanotechnology has emerged as a pivotal scientific and industrial advancement, enabling precise control over material properties at the nanoscale. Among its diverse applications, drug delivery has attracted considerable attention due to its ability to transport therapeutic agents to target sites efficiently while minimizing systemic side effects [1,2]. Nanocarriers represent one of the most advanced platforms for drug delivery, offering controlled release, enhanced therapeutic efficacy, and targeted action [3–5].

Smart nanocarriers, including polymeric nanoparticles (NPs), lipid-based NPs, dendrimers, and inorganic sites owing to their unique structural and functional features [6,7]. Among these, polymeric NPs have gained particular interest because of their biocompatibility, biodegradability into non-toxic products, and versatile biomedical applications [8,9]. Stimuli-responsive hydrogels and nanocomposites have NPs,play critical roles in delivering drugs to specific Hydrogels, composed of hydrophilic polymer networks can absorb large amounts of water while remaining insoluble in organic solvents. Their tunable swelling behavior allows precise control over drug release kinetics, making them suitable for delivering both small-molecule drugs and biomacromolecules such as proteins, peptides, and oligonucleotides [14,15]. Near-infrared (NIR)-responsive hydrogels offer advantages such as deep tissue penetration, minimal invasiveness, and selective drug release. However, conventional NIR-responsive nanocomposite hydrogels often display suboptimal photothermal efficiency [16–19]. In this study, a temperature-sensitive nanohydrogel (PPGNT) based on poly(phenylglycine) (PPG) was synthesized and evaluated primarily for its drug loading capacity, while its photothermal properties and partial drug release were also investigated, forming a stable, injectable gel suitable for localized cancer drug delivery. This system enables site-specific release upon NIR irradiation. The design of effective cancer nanotherapeutics requires careful optimization of functional particles, targeting ligands, and controlled-release mechanisms. In this work, PNPG, a biodegradable and water-soluble polymer, served as the hydrogel matrix. Its degradation into naturally occurring metabolites reduces toxicity and prolongs systemic circulation by minimizing immune recognition.

Receptor tyrosine kinases (RTKs) are key regulators of angiogenesis, tumor growth, and metastasis. Sunitinib malate (Sun), a multi-target RTK inhibitor approved by the FDA for treating renal cell carcinoma and gastrointestinal stromal tumors, demonstrates strong pharmacological and clinical performance, making it an ideal candidate for incorporation into this nanohydrogel drug delivery system [51,52].

2. Materials and methods

2.1. Chemicals and Equipment

Analytical-grade N-phenylglycine, AIBN, APS, NHS, N-vinyl caprolactam, allylamine, EDC, DMSO, α-cyclodextrin, DMF, and sulfuric acid were purchased from Sigma-Aldrich and Merck. Sun malate was kindly supplied by Sobhan Darou (Tehran, Iran). Ultrapure water was freshly prepared using a Milli-Q purification system (Millipore, USA). All reagents were used without further purification.

2.2. Structural and Morphological Characterization

FTIR: Functional groups of the synthesized nanoparticles (NPs) were identified using a PerkinElmer FTIR spectrometer (400–4000 cm^{-1}) with KBr pellet samples.

EDX: Elemental composition and mapping were analyzed using an EDX detector coupled with FE-SEM.

FE-SEM: Morphology and size distribution of the nanohydrogel and NPs were observed using a TESCAN MIRA3 microscope. Samples were sputter-coated with gold prior to imaging.

TGA: Thermal stability was evaluated using a Rheometric Scientific STA instrument over 25–600 °C at 10 °C/min under nitrogen.

UV-Vis: Absorbance measurements of Sun malate were conducted using a Cary 100 UV-Vis spectrophotometer (Agilent Technologies, USA).

2.3. Preparation of Standard Drug Solution

A stock solution of Sun was prepared at a concentration of 20 mg/L by dissolving 0.002 g of the drug in 100 mL of solvent. This stock solution was then serially diluted with deionized water to obtain standard solutions in the range of 5–80 mg/L

2.4. Synthesis and Characterization of Polyphenyl Glycine Nanoparticles

Poly(phenylglycine) (PPG) nanoparticles were prepared through oxidative polymerization of phenylglycine (PG) monomer. Briefly, 0.182 g of PG (1.2 mmol) was dissolved in 15 mL of 0.1 M sulfuric acid. Separately, 0.27 g of ammonium persulfate (APS, 1.2 mmol) was dissolved in 2 mL of 0.1 M sulfuric acid and slowly added to the monomer solution over one hour under constant stirring. The reaction mixture was maintained in an ice bath at 0–5 °C for 5 h and then stored in the dark at room temperature for 48 h. The polymer was subsequently dried under vacuum at 50 °C, resulting in a green product (Fig 1a) . To enhance functionality, PPG was further modified with allylamine, introducing reactive groups suitable for subsequent copolymerization with N-vinylcaprolactam (NVCL), yielding a temperature-sensitive nanohydrogel (PPGNT). The influence of oxidant concentration, reaction time, temperature, and pH on polymer formation was systematically evaluated [16, 27]

2.5. Characterization

The chemical structure of the synthesized polyphenyl glycine (PPG) was confirmed by Fourier-transform infrared spectroscopy (FTIR) using a Bruker IFS 66/S

instrument, with measurements taken from 400 to 4000 cm^{-1}. UV-Visible absorption spectra of PPG were recorded at ambient temperature using a Shimadzu UV-2100 spectrophotometer within the 300–900 nm wavelength range.

2.6. Synthesis of Modified Polyphenyl Glycine Nanoparticles and Characterization

Polyphenyl glycine (PPG) was functionalized with allylamine via an amide condensation reaction to produce modified PPG nanoparticles (PPGN). In detail, 0.18 g of PPG was dissolved in 20 mL of DMSO under continuous stirring at 200 rpm at room temperature (25 °C) until a clear solution was obtained (~30 min). Then, 0.31 g of EDC (2 mmol) and 0.23 g of NHS (2 mmol) were added, and the mixture was stirred for 2 hours at 25 °C under a nitrogen atmosphere to activate the carboxyl groups. Subsequently, 5 mL of allylamine was added dropwise over 5 min, and the reaction continued under nitrogen with stirring at 200 rpm for an additional 2 hours at room temperature. After that, the mixture was heated to 80 °C and kept in the dark at room temperature for 72 hours to ensure complete reaction. DMSO was removed by rotary evaporation at 10 mbar and 80 °C, with stirring at 100 rpm. The resulting dark aqueous mixture was then washed three times with deionized water to remove unreacted reagents and dried under vacuum at 50 °C for 24 hours.

The successful incorporation of allylamine functional groups into the polymer structure was confirmed by FTIR spectroscopy (range: 4000–400 cm^{-1}, resolution: 4 cm^{-1}, 32 scans; see Fig 1b).

2.7. Synthesis and Functionalization of PPGN with Temperature-Sensitive Groups

To enhance the photothermal efficiency, the modified PPG nanoparticles (PPGN) were further functionalized with temperature-sensitive groups. Briefly, 0.5 g of PPGN was dissolved in 40 mL of ethanol under continuous stirring at 200 rpm at room temperature (25 °C) until a homogeneous solution was obtained (~20 min). Then, 0.8 g of N-vinyl caprolactam, 0.1 g of AIBN (initiator), and 8 mL of allylamine were added. The monomers were added dropwise over 5 minutes, and the mixture was stirred for an additional 30 minutes at room temperature under a nitrogen atmosphere to remove dissolved oxygen and prevent radical termination.

The reaction mixture was then refluxed under nitrogen at 60–65 °C for 7 hours with continuous stirring at 200 rpm. After completion, the resulting temperature-sensitive polymer (PPGNT) was allowed to cool to room temperature and dried in a vacuum oven at 50 °C for 24 hours. Successful incorporation of temperature-sensitive groups was confirmed by FTIR spectroscopy (range: 4000–400 cm^{-1}, resolution: 4 cm^{-1}, 32 scans; see Fig 1c). Additional characterization, including SEM and TGA, was performed to assess morphology, particle size distribution, and colloidal stability .

2.8. Preparation of Sunitinib-Loaded PPGNT Nanohydrogel

Ten milliliters of Sun solution (10 mg/L) was initially dissolved in 1 mL of DMF and then diluted with 1 mL of distilled water. Subsequently, 1 mg of PPGNT was added, and the mixture was stirred at room temperature in the dark for 1 hour. After incubation, the solution was centrifuged at 3000 rpm for 15 minutes to remove any unbound Sun.The concentration of the loaded drug was determined using UV-Vis spectroscopy at λ_max = 470 nm. The drug-loaded Nanohydrogel were washed several times with deionized water and then dried at room temperature. Drug loading was calculated as the ratio of the weight of the loaded drug to the weight of the dry polymer matrix. Drug loading efficiency (DLE) was calculated using the following equation (Eq1)

$$DLE = \frac{D_e}{D_t} \cdot \frac{W}{W_0} \quad (1)$$

2.9. Preparation of Hydrogel

A total of 0.04 g of PPGNT was dissolved in 10 mL of distilled water and stirred for 15 minutes. Subsequently, 0.0001 g of Sun was added, followed by 2 mL of a 100 mg/L α-cyclodextrin (α-CD) solution. The mixture was agitated on a shaker for 15 minutes, then subjected to ultrasonic treatment for 5 minutes, and allowed to equilibrate at room temperature for a few minutes.After the adsorption process, the solution was centrifuged at 3000 rpm for 15 minutes. The concentration of Sun in the supernatant was determined using UV-Vis spectroscopy at λ_max = 470 nm. Fourier-transform infrared spectroscopy (FTIR) was performed to evaluate the degree of drug binding to the polymer matrix

2.10. Drug Release of Sunitinib under Laboratory Conditions

The release behavior of Sunitinib (Sun) under laboratory conditions was evaluated at two different pH levels, simulating physiological media: pH 7.4 (intestinal fluid) and pH 1.2 (gastric fluid). In this procedure, 0.01 g of Sun-loaded PPGNT was placed in a dialysis bag, which was immersed in the corresponding buffer solution and incubated at 37 °C with gentle shaking (50 rpm) for 30 minutes. At predetermined time intervals, the dialysis bag was removed and transferred into 5 mL of fresh buffer solution to maintain sink conditions. The amount of drug released was quantified using a UV-Vis spectrophotometer at λ_max = 470 nm. All release

experiments were performed in triplicate. The cumulative drug release percentage was calculated according to Eq(2). In this context, (Ct) and (C0) represent the amounts of Sun released and the amount of Sun loaded at time (t), respectively. The percentage of drug release can be calculated using the formula.

$$\text{Drug release (\%)} = \frac{C_t}{C_0} \times 100 \quad (2)$$

Eq(2) enables the quantitative evaluation of the cumulative release profile, providing insight into the extent of Sunitinib released from the nanohydrogel matrix over time. .

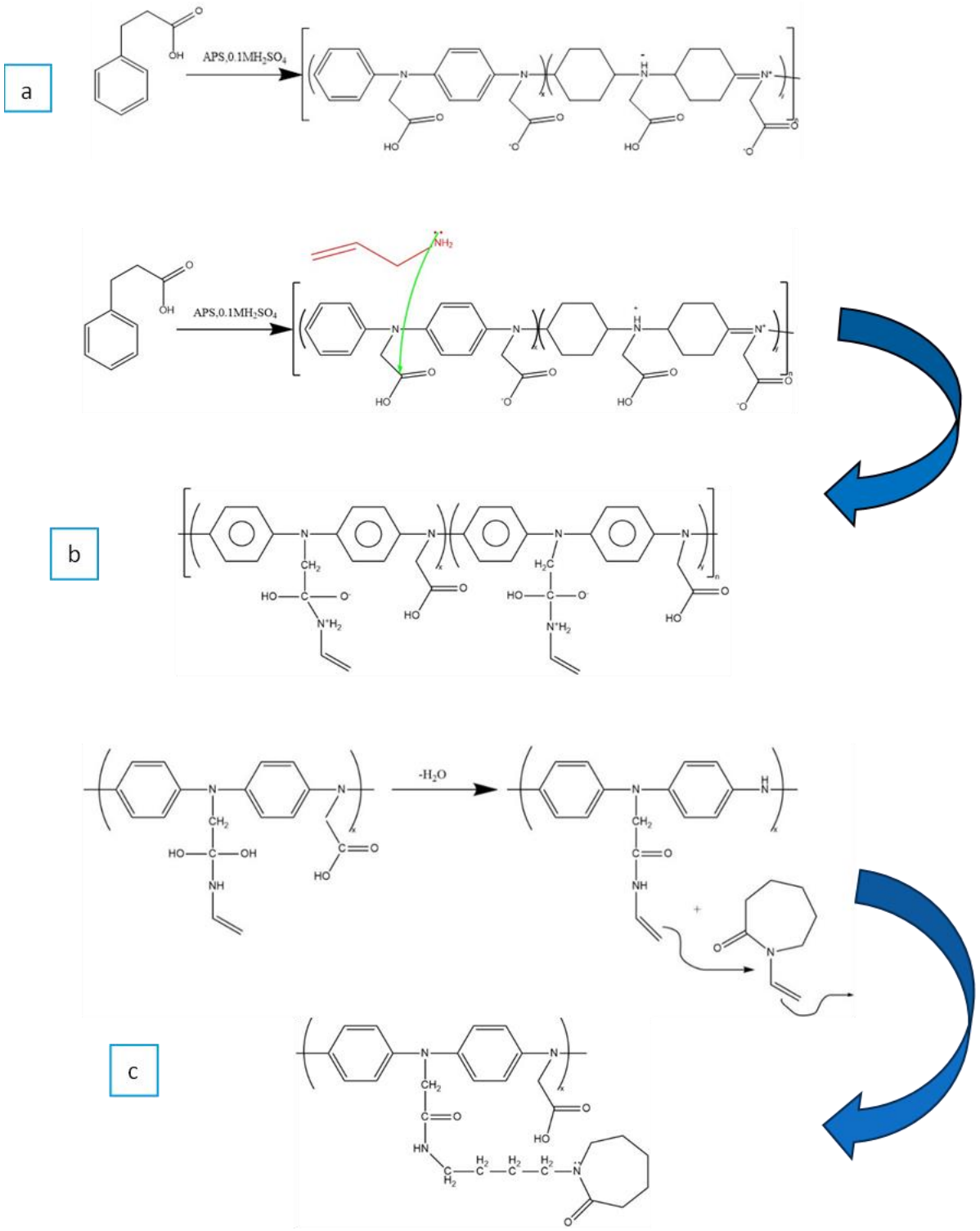

Figure 1. Schematic representation of the synthesis of (a) PPG, (b) PPGN, and (c) PPGNT

2.11. Design of Experiments Using Central Composite Design

Design of Experiments (DOE) is widely recognized as a robust approach to optimize experimental conditions while reducing the number of trials, time, and material consumption. A commonly applied strategy within DOE is Response Surface Methodology (RSM), which combines statistical and mathematical modeling to evaluate the relationships between independent variables and response outcomes.In this study, preliminary experiments identified three critical factors influencing the drug absorption of Sun by PPGNT: pH, contact time, and temperature. These factors were systematically investigated using Central Composite Design (CCD) via Design-Expert 11.0 software (Stat-Ease Inc., MN, USA). The total number of experiments was calculated according to the standard CCD equation (Eq3). This statistical approach allows for a comprehensive evaluation of both individual and interactive effects of the variables on drug loading efficiency. The results obtained from the CCD not only facilitate the determination of optimal conditions but also provide predictive models for understanding how variations in pH, contact time, and temperature affect Sun absorption. Data analysis included analysis of variance (ANOVA) to assess the significance of factors and model adequacy, with a confidence level of 95% ($p < 0.05$)

$$N=2f+2f+C_o \quad (3)$$

In Eq(3), (f) represents the number of factors considered in the design (independent variables that influence the response), and (C_0) denotes the number of central point replicates. The low and high levels for each factor are summarized in Table 1. The general second-order polynomial equation, used to model the relationship between the independent factors and the predicted response, is presented in Eq(4)

$$Y = \beta_0 + \sum_{i=1}^{k} \beta_i X_i + \sum_{i=1}^{k} \beta_{ii} X_i^2 + \sum_{i=1}^{k} \sum_{i \neq j=1}^{k} \beta_{ij} X_i X_j + \varepsilon \quad (4)$$

In this model, Y represents the predicted response, β_0 is the intercept, βi, βii and βij are the linear, quadratic, and interaction coefficients, respectively; xi and xj are the independent variables, ϵ, is the error term, and K is the total number of factors [49,50].

2.12. Adsorption Isotherms and Kinetics

Adsorption experiments were performed using Sun solutions at concentrations ranging from 5 to 80 mg/L, with a fixed amount of adsorbent, under ambient conditions. Equilibrium data were analyzed using Langmuir, Freundlich, and Temkin isotherm models, while adsorption kinetics were monitored over a time range of 2 to 60 minutes. In a representative experiment, 0.01 g of PPGNT was added to 5 mL of a 10 mg/L Sun solution at pH 7.

Table1. Experimental Levels of Factors Influencing Sun Adsorption: Contact Time, pH, and Temperature.

Variables	Code	Coded variable levels		
		-1	0	+1
pH	A	5	7	9
Contact time (min)	B	40	50	60
Temperature (°C)	C	40	50	60

To evaluate the adsorption kinetics, three models were applied: pseudo-first-order (PFO), pseudo-second-order (PSO), and intraparticle diffusion (IPD). The linear forms of the Langmuir, Freundlich, and Temkin isotherms are presented in Equations (5) , (6) , and (7) , respectively.

These models provide a comprehensive understanding of Sun's adsorption behavior on PPGNT, offering insights into both the efficiency and underlying mechanisms of drug loading on the nanoparticle matrix.

$$\frac{C_e}{q_e} = \frac{1}{K_1 \cdot q_{max}} + \frac{C_e}{q_{max}} \quad (5)$$

$$\ln q_e = \ln K_f + \frac{1}{n \cdot \ln C_e} \quad (6)$$

$$q_e = b \cdot \ln C_e + b \cdot \ln K_t \quad (7)$$

Here C_e (mg/L) is the equilibrium concentration of Sun in solution, q_e (mg/g) represents the adsorption capacity at equilibrium ,q max (mg/g) indicates the maximum adsorption capacity , K_L, K_f, and K_T are the equilibrium constants corresponding to the Langmuir, Freundlich, and Temkin isotherm models, respectively.

These parameters are essential for characterizing the adsorption process, as they provide quantitative insights into the efficiency of Sun uptake by PPGNT nanoparticles under different concentrations and experimental conditions.

Accurate determination of these values facilitates optimization of the drug delivery system and prediction of its performance in practical applications These parameters are crucial for characterizing the adsorption process, allowing for the assessment of how effectively the drug is being adsorbed onto the PPGNT nanohydrogel at various concentrations and conditions. Understanding these values aids in optimizing the drug delivery system and predicting its behavior in practical applications.

3. Conclusion and Discussion

3.1. Characterization

3.1.1. *FTIR Analysis*

The successful synthesis of PPG, PPGN, and PPGNT was confirmed by FTIR analysis (Fig 2) . For PPG, the characteristic absorption peaks at 1580 cm^{-1} and 1498 cm^{-1} correspond to quinonoid and benzenoid rings, respectively. Upon modification with allyl amine, these bands shifted to 1556 cm^{-1} and 1467 cm^{-1} in PPGN, indicating effective functionalization of the polymer backbone.FTIR spectra of PPGNT loaded with Sun and Sun–α-Cyclodextrin (Fig 3) exhibited absorption bands at 3300 cm^{-1} and 2800 cm^{-1}, corresponding to the N–H stretching of amino groups, while bands at 1600 cm^{-1} and 1500 cm^{-1} were attributed to conjugated alkenes and nitro groups. Additionally, peaks at 1000 cm^{-1}, 800 cm^{-1}, and 600 cm^{-1} were assigned to alkene stretching and halide vibrations, confirming successful drug loading onto the nanocarrier.These spectral changes not only validate the stepwise chemical modifications from PPG to PPGNT but also indicate strong interactions between the polymer matrix and SUN, which are likely to enhance drug encapsulation and stability. The shifts in key functional group vibrations suggest potential hydrogen bonding and π–π interactions between Sun and the modified polymer, which can positively influence the drug release profile and adsorption efficiency. This observation aligns with previous studies reporting that functionalization of polymeric carriers improves drug–carrier interactions and overall loading capacity.

3.1.2. *SEM-EDX Analysis*

SEM analysis was employed to investigate the morphology and surface characteristics of the synthesized nanoparticles. The micrographs revealed that the particles were interspersed between layers, forming polymeric agglomerates with sizes below 100 nm. Particle sizes are indicated in the Fig 4a with dimensions of 20, 30, 40, 50, and 60 nm. The surface of these agglomerates appeared rough and porous, providing abundant cavities that facilitate drug adsorption.Fig 4 presents SEM images at two stages of polymer preparation (initial and after functionalization with amino and temperature-sensitive groups). The images clearly demonstrate that surface modification increased the number and size of surface pores and cavities. This structural enhancement improved the porosity and heterogeneity of the particles, which is critical for enhancing the adsorption capacity and functionality of the nanoparticles.

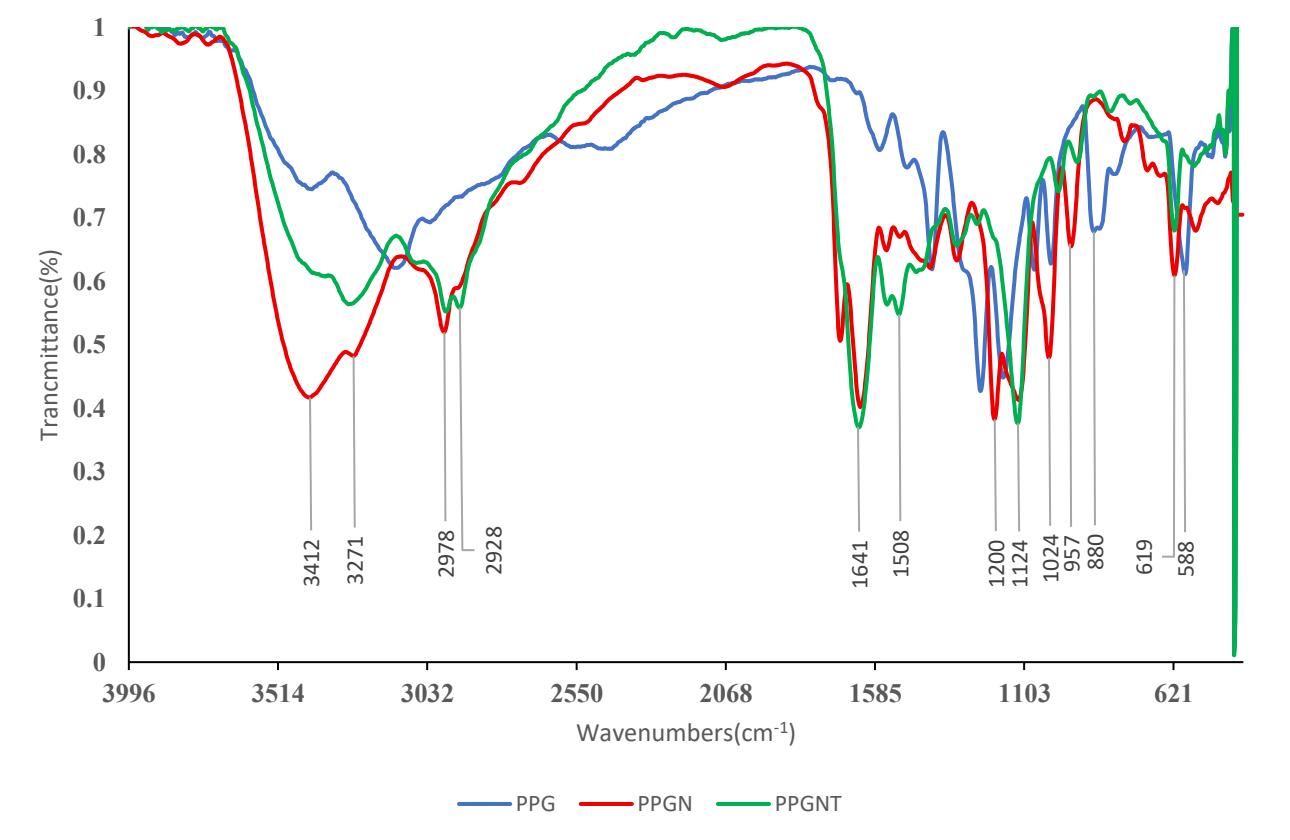

Figure 2. FT-IR spectra of PPG, PPGN, and PPGNT, showing key functional groups and confirming stepwise polymer modification and drug loading

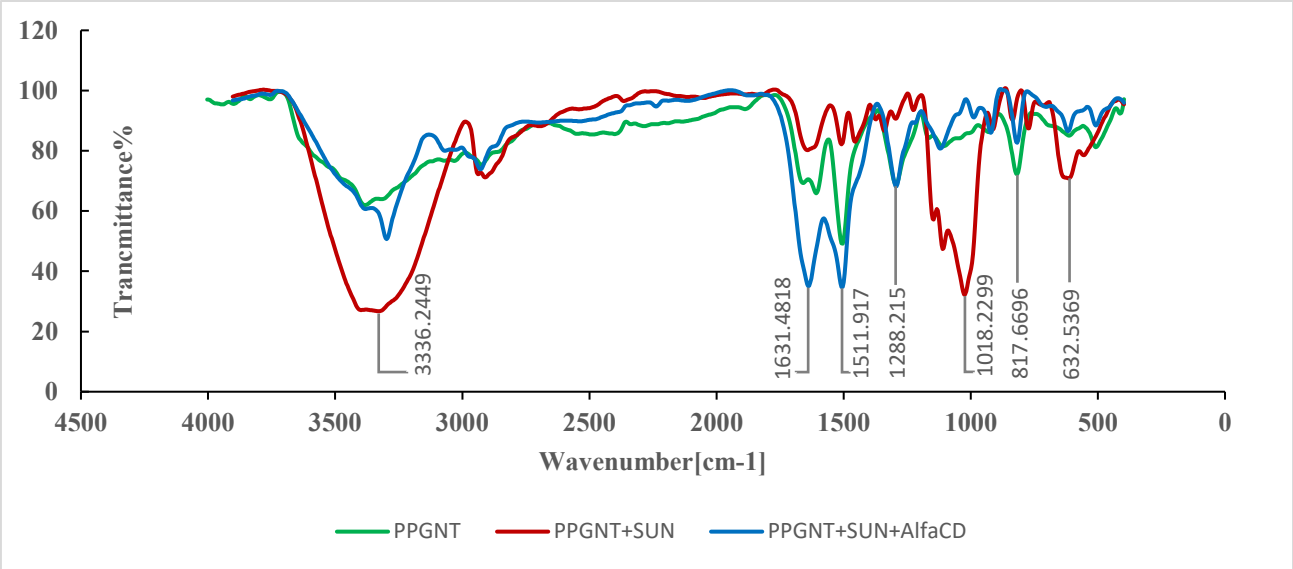

Figure 3. FT-IR spectra of PPGNT, PPGNT–Sun, and PPGNT–Sun–αCD, highlighting key functional groups and confirming successful drug loading and complexation with α-cyclodextrin.

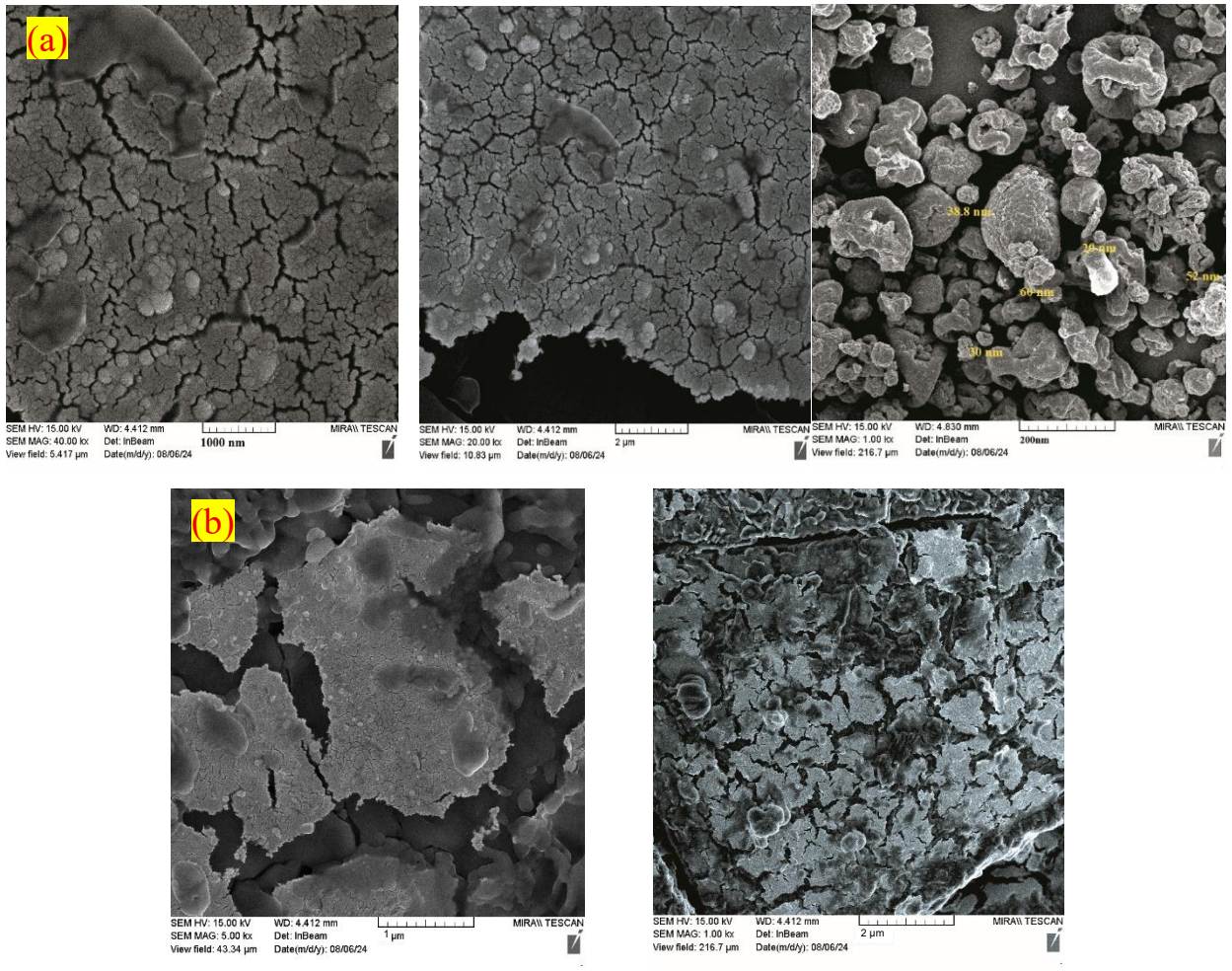

Figure 4. SEM images of (a) PPGNT and (b) PPGNT-SUN, showing particle morphology, surface roughness, and porous structure contributing to drug loading capacity.

EDX analysis (Table 2) confirmed the successful surface modification of the nanoparticles. The spectrum showed increased levels of oxygen, carbon, and nitrogen after the incorporation of ethanol, allyl amine, and vinyl

caprolactam, indicating the formation of light- and temperature-sensitive functional groups on the polymer substrate

3.1.3. *Thermogravimetric Analysis (TGA)*

As shown in the thermal analysis spectrum (Fig 5A), the synthesized polymeric nanohydrogel exhibits an initial weight loss of about 5% at 100 °C, mainly attributed to the evaporation of residual moisture. Between 100 °C and 200 °C, an additional 20% loss is related to the removal of surface-adsorbed water. A major degradation step occurs between 200 °C and 300 °C, where approximately 50% weight loss is observed due to decomposition of the polymer backbone.

Table 2. Percentages of elements detected in the synthesized nanoparticles based on EDX spectrum obtained from FESEM analysis

Elements	Weight Percentages in the First Stage	Weight Percentages in the Third Stage
Oxygen	10.9	12.28
Carbon	66.49	57.77
Nitrogen	24.82	62.86

The final degradation stage, detected in the range of 400–600 °C, accounts for about 15% weight loss and is assigned to the breakdown of nanoparticle chains. Fig 5B illustrates the thermal behavior of the nano-adsorbent modified with amino groups and temperature-sensitive moieties. Unlike the unmodified polymer, the modified sample shows an earlier onset of degradation around 70 °C, highlighting its enhanced temperature sensitivity. At 100 °C, nearly 90% of the polymeric structure remains intact, while between 100 °C and 220 °C, an additional weight loss of approximately 20% is attributed to the removal of surface-bound water. Beyond 200 °C, a sharp weight reduction confirms the progressive thermal degradation of the polymer backbone in the temperature-responsive nanoparticles

3.2. Optimization of Adsorption Conditions Using Experimental Design (CCD Model)

The influence of three critical factors, including pH, contact time, and temperature, on the adsorption of Sun by the synthesized Nanohydrogel was systematically investigated using a Central Composite Design (CCD) model. Each parameter was studied at three levels, and based on the experimental design, a total of 20 runs were generated by the software. The experimental data were then compared with the predicted values obtained from the CCD model to evaluate the model's accuracy.

As presented in Table 3, the maximum adsorption efficiency was achieved under the conditions of pH 7, contact time of 50 min, and temperature of 60 °C. All experiments were conducted in triplicate, and the mean values were calculated and reported. The relationship between adsorption efficiency and the studied variables was expressed by a second-order polynomial equation (Eq 8)

$$R = -365+1.46C+51.56B+8.82^{a} - 0.0067C^{2}-3.572B^{2}-0.0828A^{2} - 0.053CB-0.0024CA-0.011BA \quad (8)$$

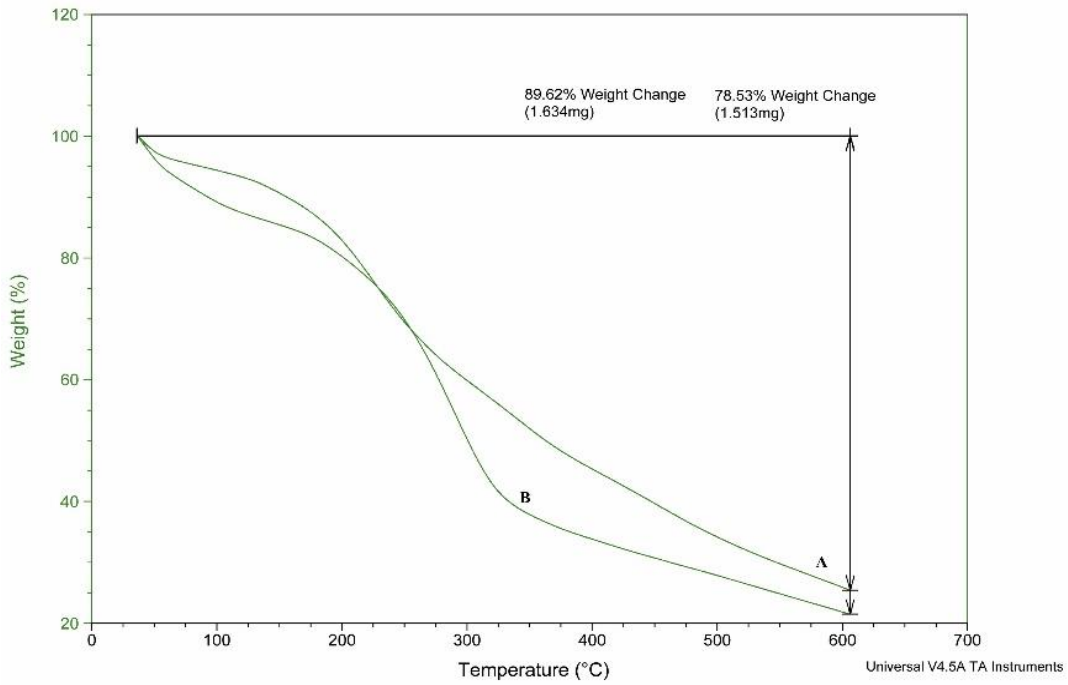

Figure 5. TGA spectrum of the synthesized polymeric Nanohydrogel, showing multi-step weight loss corresponding to moisture evaporation, removal of volatile compounds, and polymer backbone degradation.

3.3. Statistical Calculations

Analysis of variance (ANOVA) was employed to evaluate the statistical significance of the investigated factors. As summarized in Table 4, the variables of pH, contact time, and temperature exhibited a significant influence on Sun adsorption by the PPGNT nanohydrogel, with p-values < 0.05 at a 95% confidence interval. The high F-value (98.07, $p < 0.0001$) further confirmed the robustness of the regression model. The obtained R^2, adjusted R^2, and predicted R^2 values were all within acceptable ranges, supporting the adequacy and reliability of the quadratic model. The diagnostic plots in Fig 6 provide additional verification of model assumptions. The normal probability plot of residuals (Fig 6a) indicated that most points aligned closely with the reference line, suggesting residual normality. Residuals versus fitted values plot (Fig 6b) displayed a uniform distribution of residuals around zero, confirming homoscedasticity. The histogram of residuals (Fig 6c) further supported the assumption of normally distributed errors. Finally, Residuals versus observation order plot (Fig 6d) demonstrated strong agreement between experimental and predicted responses, confirming the model's predictive accuracy with only minor deviations. Collectively, these statistical evaluations validate that the CCD-based quadratic model reliably describes the adsorption behavior of Sun onto the PPGNT nanohydrogel.

Table 3. Experimental Results and Predicted Values for Sun Adsorption Optimization Using CCD Model

Std	Run	Block	A:pH	time(Min) B:Contact	C=Temperature(°C)	RECOVERY%	
						Predicted	Actual
9	1	Block1	5	60	60	66.43	65.45
4	2	Block1	5	40	40	57.20	56.89
7	3	Block1	5	40	60	66.43	64.32
1	4	Block1	5	60	40	57.63	58.96
6	5	Block1	9	60	60	50.93	53.50
10	6	Block1	9	60	40	52.38	51.24
8	7	Block2	9	40	40	51.21	50.02
2	8	Block2	7	50	50	82.00	74.22
5	9	Block2	9	40	60	50.55	53.25
3	10	Block2	7	50	50	79.21	74.53
12	11	Block2	7	50	50	86.22	86.22
11	12	Block2	7	50	50	86.22	86.00
20	13	Block3	7	50	50	84.29	85.88
16	14	Block3	7	50	60	89.73	91.42
15	15	Block3	7	50	50	84.29	86.12
19	16	Block3	7	50	50	52.28	50.17
14	17	Block3	9	40	50	52.38	51.76
13	18	Block3	5	50	40	82.00	78.43
18	19	Block3	7	50	50	44.36	46.87
17	20	Block3	7	60	50	80.00	77.34

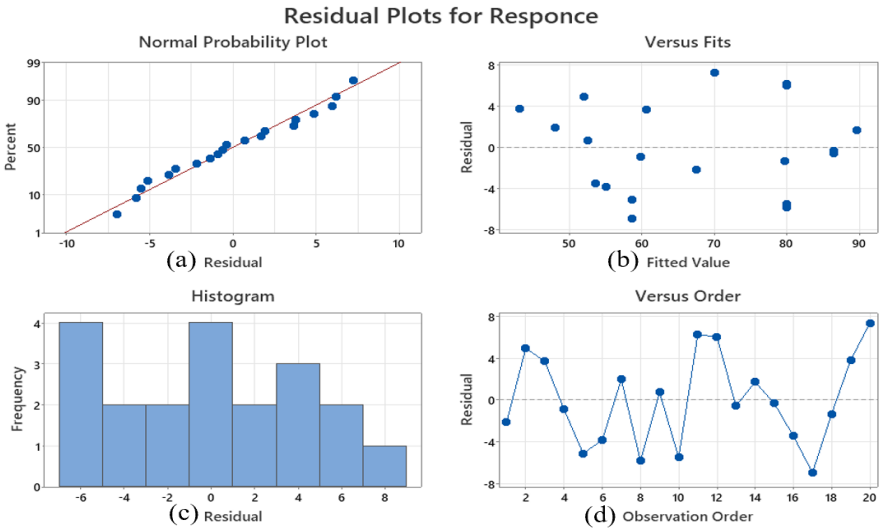

Figure 6. Statistical diagnostic plots for Sun adsorption on the PPGNT Nanohydrogel: (a) Normal probability plot of residuals, (b) Residuals versus fitted values plot, (c) Histogram of residuals, and (d) Residuals versus observation order plot.

Table 4. ANOVA results for the adsorption efficiency of Sun on PPGNT Nanohydrogel.

Source	Sum of Squares	df	Mean Square	F-value	p-value	
Block	728.58	2	364.29			
Model	5229.00	9	581.00	98.07	< 0.0001	significant
A-pH	213.07	1	213.07	35.96	0.0003	
B-Contact time	883.22	1	883.22	149.08	< 0.0001	
C-Temperature	303.38	1	303.38	51.21	< 0.0001	
AB	2.81	1	2.81	0.4740	0.5106	
AC	3.62	1	3.62	0.6107	0.4570	
BC	0.8844	1	0.8844	0.1493	0.7093	
A^2	1356.02	1	1356.02	228.88	< 0.0001	
B^2	366.58	1	366.58	61.87	< 0.0001	
C^2	0.0118	1	0.0118	0.0020	0.9655	
Residual	47.40	8	5.92			
Lack of Fit	42.23	5	8.45	4.90	0.1105	not significant
Pure Error	5.17	3	1.72			
Cor Total	6004.97	19				
R^2=0.9910						
R^2_{adj}=0.9809						
R^2 (predict)=0.8706						

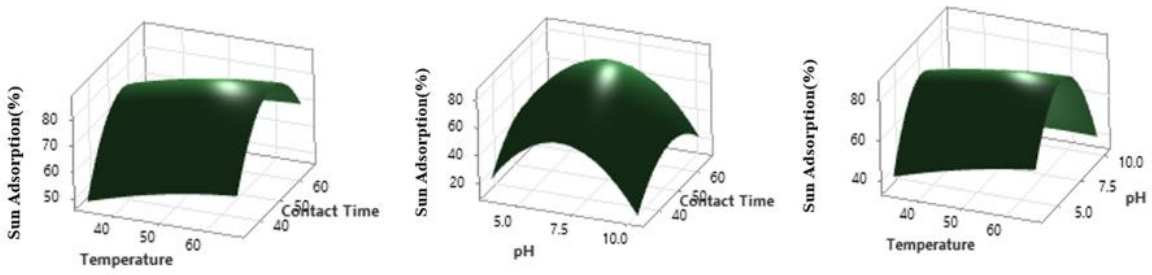

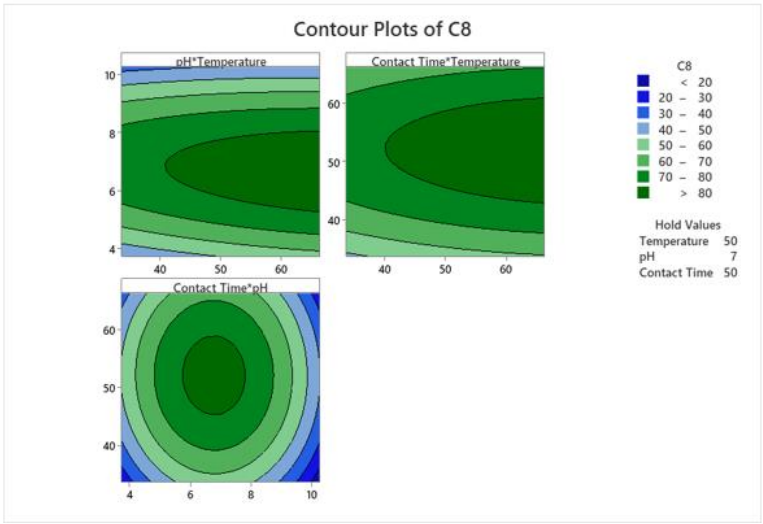

Figure 7. Contour and 3D response surface plots illustrating the interaction effects of pH, contact time, and temperature on the adsorption of Sun by the PPGNT nanohydrogel

Analysis of Contour Plots (2D and 3D)

The 2D contour and 3D response surface plots (Figure 7) illustrate the interaction effects of pH, contact time, and temperature on Sun adsorption by PPGNT. Maximum adsorption (~90%) was achieved at pH 8, contact time 50 min, and moderate temperature. Increasing pH and contact time generally enhanced adsorption, while further increases in temperature reduced it. The plots highlight the combined effects of two variables at a time, indicating optimal conditions for drug uptake.

3.4. Adsorption Isotherms and Kinetics

3.4.1. *Adsorption Isotherms of Sun on PPGNT Nanohydrogel*

The equilibrium data of Sun adsorption on PPGNT were analyzed using Langmuir, Freundlich, and Temkin models (Table 5) . The Langmuir model showed the best fit (R^2 = 0.996), indicating monolayer adsorption. The separation factor (RL = 0.623) and Freundlich 1/n value ($0 < 1/n < 1$) confirm that adsorption is favorable, while the positive Temkin B parameter suggests an exothermic process .

3.5. Adsorption Kinetics

3.5.1 *Adsorption Kinetics of Sun on PPGNT Nanohydrogel*

The adsorption kinetics of Sun onto PPGNT were evaluated using pseudo-first-order (PFO), pseudo-second-order (PSO), and intraparticle diffusion (IPD) models (Table 6) . The PSO model provided the best fit, with a correlation coefficient of 0.992, indicating that the adsorption process is primarily governed by chemisorption. The IPD model showed a multi-stage behavior, suggesting that the adsorption involves an initial rapid uptake on the adsorbent surface followed by slower diffusion into the pores, but intraparticle diffusion is not the rate-limiting step.

Table 5. Isotherm model parameters calculated using the linear method.

Isotherm model	Parameter	Quantity	R^2
Langmuir	qm (mg g -1) KL (L mg -1) RL	9.224 0.010 0.532	0.996
Freundlich	KF (mg g-1) (Lmg -1)1/n n	0.108 0.001	0.995
Temkin	A (L mg-1) B (J mol-1)	0.218 1.158	0.987

Table 6. Parameters of kinetic adsorption of sunitinib (Sun) by the PPGNT nanohydrogel

Model	Parameter	Value
Pseudo-first-order model	q_e(mg/g) k_1(min^{-1}) R^2	0.976 0.163 0.901
Pseudo-second-order model	q_e(mg/g) k_2(g/mgmin) R^2	1.246 0.297 0.992

3.6. In Vitro Drug Release

The release of Sun from the Nanohydrogel was evaluated in simulated intestinal (pH 7.4) and gastric (pH 1.2) environments (Fig 8) . In the intestinal condition, ~10% of the drug was released within the first 30 min, followed by a slower release reaching ~50% over the study period. In the gastric environment, the release was faster, with 28% released in the first 30 min and ~90% after 5 h.

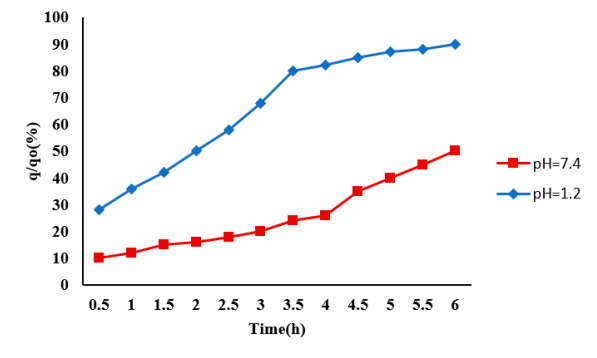

Figure 8. Drug release profile under in vitro conditions at 37 °C over 6 hours.

3.7. Method Validation

The proposed analytical method was validated using standard Sun samples. Linearity was assessed over a concentration range of 0.62–50 µg/mL, yielding a correlation coefficient (R^2) of 0.998. The method's reproducibility and repeatability were evaluated through three independent measurements on different days, with low relative standard deviations (RSD). The limit of detection (LOD) and limit of quantification (LOQ) were determined as 6.12 and 18.6 ng/mL, respectively. These results confirm that the method is reliable, accurate, and suitable for quantifying Sun in the prepared samples.

4. Conclusion

Hydrogels are highly promising materials for controlled and targeted drug delivery due to their ability to retain bioactive agents within their swollen polymeric networks. Advances in chemistry and nanotechnology have enabled the development of smart hydrogel-based nanocarriers capable of site-specific and stimulus-responsive drug release. Over time, these systems have evolved from simple single-component hydrogels to complex multi-component networks, providing controlled release in response to environmental stimuli. In this study, a temperature and UV-responsive nanohydrogel (PPGNT) based on poly(phenylglycine) (PPG) was successfully synthesized and modified with crosslinking and biologically reactive groups. The polymeric base demonstrated excellent photothermal efficiency and stability compared to similar nanocomposites reported in the literature, with responsiveness to near-infrared (NIR) light. The nanohydrogel efficiently adsorbed and delivered the drug Sun (sunitinib malate) to the target site.

Characterization using FT-IR, FE-SEM, and TGA confirmed the successful synthesis and surface modification of the nanoparticles. Adsorption studies revealed that the drug loading followed pseudo-second-order kinetics and a Langmuir isotherm model, indicating monolayer adsorption on uniform sites. Optimization of adsorption parameters using RSM and CCD models further highlighted the effective interaction between the drug and nanocarrier.

In vitro release studies in simulated gastric (pH 1.2) and intestinal (pH 7.4) conditions at 37 °C over 6 hours demonstrated controlled and stimulus-responsive drug release. Method validation showed excellent sensitivity, accuracy, precision, and reproducibility, with LOD and LOQ values supporting the reliability of the proposed approach. Additionally, the nanohydrogel exhibited reusability over several consecutive adsorption cycles, confirming its practical applicability.

Overall, the synthesized nanohydrogel not only provides a smart and effective platform for targeted drug delivery to cancer cells but also, due to its photothermal polymeric base, offers the potential for enhanced therapeutic effects with minimal side effects. This work demonstrates the advantages of integrating adsorption capacity, controlled release, and stimulus responsiveness into a single polymeric system, providing a foundation for future development of advanced drug delivery platforms.

Table 7. Comparison of the Proposed Nanohydrogel for Sunitinib Malate Delivery with Other Nanocarriers

Nanocarrier Type	Encapsulation Efficiency (EE%)	Drug Release	pH / Stimulus Sensitivity	Drug Loading Time	Loading Temp (°C)	Reference
Eudragit S-100 NP (ESNPF2)	60.3 %	At pH 7.4 , 10.2 % at 4 h , 66.5 % at 12 h , 82.2 %	Colon-targeted, pH-dependent (optimized release at pH 7.4)	12 h stirring at room temp	room temp25° C	Jamil et al. (2024)
Hydrogel/CMC–Cloisite 30B (~6 wt%)	93 % (vs. 81 % without Cloisite)	240 min study: • Release higher at pH 7.4 than 5.5	pH-responsive hydrogel; higher swelling & release at pH 7.4	24 h swelling/diffusion	25-37°C	BMC Biotechnol. (2025)
methacrylic acid and ethylene glycol dimethacrylate	76%	rebinding percentage was 70%	optimized release at pH 7.4	24 h	37 ◦C	[49]
Methoxy-hypromellose-based polymeric NP (mHPMC)	>86 %	High capacity; minimal release at pH 7.4	pH-responsive, release increases in acidic tumor microenvironment	Overnight mixing (~12–16 h)	25-30◦C	Teaser in ScienceDirect

References

[1] Hussain SMM, Ladha BZ, Khan MH. Nanotechnology: arevolution in modern industry. Molecules. 2023;28(2):661. doi:10.3390/molecules28020661.

[2] Kanaoujiya R, Saroj SK, Rajput VD, Alimuddin, Srivastava S, Minkina T, et al. Emerging application of nanotechnology for mankind. Emergent Mater. 2023;6(2):439–52. doi:10.1007/s42247-023-00461-8.

[3] Islam S, Ahmed MMS, Islam MA, Hossain N, Chowdhury MA. Advances in nanoparticles in targeted drug delivery: a review. Results Surf Interfaces. 2025;19:100529. doi:10.1016/j.rsurfi.2020.100529.

[4] Cong X, Zhang Z, Li H, Yang YG, Zhang Y, Sun T. Nanocarriers for targeted drug delivery in the vascular system: focus on endothelium. J Nanobiotechnol. 2024;22:620. doi:10.1186/s12951-024-02892-9.

[5] Zhao Z, Ukidve A, Kim J, Mitragotri S. Targeting strategies for tissue-specific drug delivery. Cell. 2020;181(1):151–67. doi:10.1016/j.cell.2020.02.001.

[6] Kenchegowda M, Rahamathulla M, Hani U, Begum MY,

Guruswamy S, Osmani RAM, et al. Smart nanocarriers as an emerging platform for cancer therapy: a review. Molecules. 2022;27(1):146. doi:10.3390/molecules27010146.

[7] Torabi Fard N, Tadayon F, Ahmad Panahi H, Moniri E. Synthesis, characterization and application of a novel three-dimensional magnetic graphene oxide decorated with polyester dendrimers for detection of donepezil hydrochloride in pharmaceutical formulation and biological fluid. Journal of Molecular Liquids. 2022;365:118149. doi:10.1016/j.molliq.2021.118149.

[8] Pires PC, Mascarenhas-Melo F, Pedrosa K, Lopes D, Lopes J, Macário-Soares A, et al. Polymer-based biomaterials for pharmaceutical and biomedical applications: a focus on topical drug administration. European Polymer Journal. 2023;187:111868. doi:10.1016/j.eurpolymj.2023.111868.

[9] Liechty WB, Kryscio DR, Slaughter BV, Peppas NA. Polymers for drug delivery systems. Annu Rev Chem Biomol Eng. 2010;1:149–73. doi:10.1146/annurev-chembioeng-073009-100847.

[10] Wang T, Wu C, Hu Y, Zhang Y, Ma J. Stimuli-responsive nanocarrier delivery systems for Pt-based antitumor complexes: a review. RSC Adv. 2023;13:16488–511. doi:10.1039/D3RA00866E.

[11] Rahmaninia M, Tamaddon AM, Yazdani M, Sameni J. Cytotoxicity and in vitro evaluation of whey protein-based hydrogels. Int J Ind Chem. 2019;10(3):341–50. doi:10.1007/s40090-019-0181-3.

[12] Ahmadian I, Kargar Razi M, Sadeghi B, Nakhaei M. Synthesis of photocatalytic material based on polyaniline supported PVC/$NiAl_2O_3$/AlF_3 nanocomposite. Int J Ind Chem. 2024;15(2):16. doi:10.57647/j.ijic.2024.1502.16.

[13] Nosrati H, Heydari M, Khodaei M. Cerium oxide nanoparticles: synthesis methods and applications in wound healing. Mater Today Bio. 2023;23:100823. doi:10.1016/j.mtbio.2023.100823.

[14] Rajaram S, Dharmalingam SR, Natarajan V, Ravi K, Shanmugam N. An extensive review on hydrogels in pharmaceutical drug delivery applications. Int J Pharm Investig. 2022;12(2):108–12. doi:10.5530/ijpi.2022.2.20.

[15] Hoare TR, Kohane DS. Hydrogels in drug delivery: progress and challenges. Polymer. 2008;49(8):1993–2007. doi:10.1016/j.polymer.2008.01.027.

[16] Liu C, Guo X, Ruan C, Hu H, Jiang BP, Liang H, et al. An injectable thermosensitive photothermal-network hydrogel for near-infrared-triggered drug delivery and synergistic photothermal-chemotherapy. Acta Biomater. 2019;96:281–94. doi:10.1016/j.actbio.2019.07.024.

[17] Yu Y, Cheng Y, Tong J, Zhang L, Wei Y, Tian M. Recent advances in thermo-sensitive hydrogels for drug delivery. J Mater Chem B. 2021;9:2979–92. doi:10.1039/D0TB02877K.

[18] Salehi S, Naghib SM, Garshasbi HR, Ghorbanzadeh S, Zhang W. Smart stimuli-responsive injectable gels and hydrogels for drug delivery and tissue engineering applications: a review. Front Bioeng Biotechnol. 2023;11:1104126. doi:10.3389/fbioe.2023.1104126.

[19] Li J, Mooney DJ. Designing hydrogels for controlled drug delivery. Nat Rev Mater. 2016;1(12):16071. doi:10.1038/natrevmats.2016.71.

[20] Torabi Fard N, Tadayon F, Ahmad Panahi H, Moniri E. The synthesis of functionalized graphene oxide by polyester dendrimer as a pH-sensitive nanocarrier for targeted delivery of venlafaxine hydrochloride: central composite design optimization. J Mol Liq. 2021;349:118149. doi:10.1016/j.synthmet.2022.117141.

[21] Zhang XZ, Zhuo RX, Cui JZ, Zhang JT. A novel thermo-responsive drug delivery system with positive controlled release. J Pharmaceutics. 2002;235:43–50. doi:10.1016/S0378-5173(01)00976-0.

[22] Bae YH, Okano T, Hsu R, Kim SW. Thermosensitive polymers as on–off switches for drug release. Chem Rapid Commun. 1987;8:481–5. doi:10.1002/marc.1987.030081002.

[23] Rahimi Haji Abadi F, Tadayon F, Tehrani MS, Ahmad Panahi H. Synthesis and characterization of the photoresponsive and thermoresponsive molecularly imprinted polymer with a novel functional monomer for controlled release of 4-aminopyridine. Int J Polym Mater Polym Biomater. 2023;72(6):425–32. doi:10.1080/00914037.2021.2018318.

[24] Shi X, Gong H, Li Y, Wang C, Cheng L, Liu Z. Graphene-based magnetic plasmonic nanocomposite for dual bioimaging and photothermal therapy. Biomaterials. 2013;34:4786–93. doi:10.1016/j.biomaterials.2013.03.046.

[25] Cheng L, Yang K, Chen Q, Liu Z. Organic stealth nanoparticles for highly effective in vivo near-infrared photothermal therapy of cancer. ACS Nano. 2012;6:5605–13. doi:10.1021/nn302236d.

[26] Jiang B-P, Zhang L, Guo X-L, Shen X-C, Wang Y, Zhu Y, Liang H. Poly(N-phenylglycine)-based nanoparticles as highly effective and targeted near-infrared photothermal therapy/photodynamic therapeutic agents for malignant melanoma. J Nanomicro Small. 2016;13(8):1602496. doi:10.1002/smll.201602496.

[27] Nabid MR, Taheri SS, Sedghi R, Entezami AA. Chemical synthesis and characterization of water-soluble, conducting poly(N-phenylglycine). Iranian Polymer J. 2008;17(5):365–71.

[28] Mubarak ANM, Naseem K, Tabassum H, Rizwan M, Najda A, Kashif M, et al. Recent advancement and development of chitin and chitosan-based nanocomposite for drug delivery: critical approach to clinical research. Arab J Chem. 2020;13:8935–64. doi:10.1016/j.arabjc.2020.10.003.

[29] Kumari S, Singh RP, Chavan NN, Sahi SV, Sharma N. Characterization of a novel nanocomposite film based on functionalized chitosan–Pt–Fe_3O_4 hybrid nanoparticles. Nanomaterials. 2021;11:1275. doi:10.3390/nano11051275.

[30] Fang G, Yang X, Chen S, Wang Q, Zhang A, Tang B. Cyclodextrin-based host–guest supramolecular hydrogels for local drug delivery. J Coord Chem Rev. 2022;454:214352. doi:10.1016/j.ccr.2022.214352.

[31] Hamidi M, Azadi A, Rafiei P. Hydrogel nanoparticles in drug delivery. Adv Drug Deliv Rev. 2008;60:1638–49. doi:10.1016/j.addr.2008.08.002.

[32] Amin S, Rajabnezhad S, Kohli K. Hydrogels as potential drug delivery systems. Sci Res Essay. 2009;3:1175–83.

[33] Ichikawa H, Fukumori Y. Design of nanohydrogel-incorporated

microcapsules for appropriate controlled-release of peptide drugs. Yakugaku Zasshi. 2007;127:813–23. doi:10.1248/yakushi.127.813.

[34] Lee SM, Yoo ES, Ghim HD, Lee SJ. Alginate nanohydrogels prepared by emulsification-diffusion method. Macromol Res. 2009;17:168–73. doi:10.1007/BF03218674.

[35] Jahanbekam S, Asare-Addo K, Alipour S, Nokhodchi A. Smart hydrogels and the promise of multi-responsive in-situ systems. J Drug Deliv Sci Technol. 2025;107:106758. doi:10.1016/j.jddst.2025.106758.

[36] Stevanović N, Filipović N. A review of recent developments in biopolymer nano-based drug delivery systems with antioxidative properties: insights into the last five years. Pharmaceutics. 2024;16(5):670. doi:10.3390/pharmaceutics16050670.

[37] Patra JK, Das G, Fraceto LF, Campos EVR, Rodriguez-Torres MdP, Acosta-Torres LS, et al. Nano based drug delivery systems: recent developments and future prospects. Nanobiotechnol. 2018;16:71. doi:10.1186/s12951-018-0392-8.

[38] Hoffman AS. The origins and evolution of controlled drug delivery systems. J Control Release. 2008;132(3):153–63. doi:10.1016/j.jconrel.2008.08.012.

[39] Masood F. Polymeric nanoparticles for targeted drug delivery system for cancer therapy. Mater Sci Eng C. 2016;60:569–78. doi:10.1016/j.msec.2015.11.067.

[40] Pinto Reis C, Neufeld RJ, Ribeiro AJ, Veiga F. Nanoencapsulation I. Methods for preparation of drug-loaded polymeric nanoparticles. Nanomedicine. 2006;2:8–21. doi:10.1016/j.nano.2005.12.003.

[41] Anwar M, Afzal I, Abid H, Ullah I, Haq UU. Nanoparticles in drug delivery: a chemical engineering perspective on biocompatibility targeting and controlled release mechanisms. Kashf J Multidiscip Res. 2025;2(03):27–46. doi:10.71146/kjmr337

[42] Hosny S, Mohamed LZ, Ragab MS, Alomoush QK, Abdalla EM, Aly SA. Nanomaterials in biomedical applications: opportunities and challenges—a review. Chem Pap. 2025;79:2657–78. doi:10.1007/s11696-025-03937-5.

[43] Abu-Thabit NY. Chemical oxidative polymerization of polyaniline: a practical approach for preparation of smart conductive textiles. J Chem Educ. 2017;93(9):94–101. doi:10.1021/acs.jchemed.6b00060.

[44] Chen H, Liang W, Zhu Y, Guo Z, Jian J, Jiang B-P, et al. Supercharged fluorescent protein functionalized watersoluble poly(N-phenylglycine) nanoparticles for highly effective imaging-guided photothermal therapy. Chem Commun. 2018;54:73. doi:10.1039/C8CC05278F.

[45] Pham DT, Nguyen DX, Nguyen NY, Nguyen TTL, Nguyen TQC, Vo TT, Nguyen NH, Thuy BTP. Development of pH-responsive Eudragit S100-functionalized silk fibroin nanoparticles as a prospective drug delivery system. PLoS ONE. 2024;19:e0303177. doi:10.1371/journal.pone.0303177.

[46] Sayyar Z, Mohammadzadeh Pakdel P, Peighambardoust SJ. Oral delivery of sunitinib malate using carboxymethyl cellulose/poly(acrylic acid-itaconic acid)/Cloisite 30B nanocomposite hydrogel as a pH-responsive carrier. BMC Biotechnol. 2024;24:70. doi:10.1186/s12896-024-00883-0.

[47] Scrivano L, Parisi OI, Iacopetta D, Ruffo M, Ceramella J, Sinicropi MS, Puoci F. Molecularly imprinted hydrogels for sustained release of sunitinib in breast cancer therapy. Polym Adv Technol. 2018;30(3):743–8. doi:10.1002/pat.4512.

[48] Jafari H, Mahdavinia GR, Kazemi B, Ehrlich H, Joseph Y, Rahimi N, Nasrabadi. Highly efficient sunitinib release from pH-responsive mHPMC@Chitosan core-shell nanoparticles. Carbohydr Polym. 2021;258:117719. doi:10.1016/j.carbpol.2021.117719.

[49] Tunç ID, Erol M, Günes F, Sütçü M. Growth of ZnO nanowires on carbon fibers for photocatalytic degradation of methylene blue aqueous solutions: An investigation on the optimization of processing parameters through response surface methodology/central composite design. Ceram Int. 2020;46:7459–74. doi:10.1016/j.ceramint.2019.11.244.

[50] Zhang B, Han X, Gu P, Fang S, Bai J. Response surface methodology approach for optimization of ciprofloxacin adsorption using activated carbon derived from the residue of desilicated rice husk. J Mol Liq. 2017;238:316–25. doi:10.1016/j.molliq.2017.04.022.

[51] Hao Z, Sadek I. Sunitinib: the anti-angiogenic effects and beyond. OncoTargets and Therapy. 2016;9:5495–5505. https://doi.org/10.2147/OTT.S112242.

[52] Kim S., Ding W., Zhang L., et al. Clinical response to sunitinib as a multitargeted tyrosine-kinase inhibitor (TKI) in solid cancers: a review of clinical trials. OncoTargets and Therapy. 2014;7:719–728. https://doi.org/10.2147/OTT.S61388.